

Transdermal hydrogen sulfide delivery enabled by open metal site metal-organic frameworks

Ruth M. Mandel,^{a,‡} Piyusha S. Lotlikar,^{a,‡} Tomče Runčevski,^b Jung-Hoon Lee,^c Joshua J. Woods,^{a,d,†} Tristan A. Pitt,^a Justin J. Wilson,^a Phillip J. Milner ^{a,*}

^aDepartment of Chemistry and Chemical Biology, Cornell University, Ithaca, NY 14850, United States

^bDepartment of Chemistry, Southern Methodist University, Dallas, TX 75275, United States

^cComputational Science Research Center, Korea Institute of Science and Technology (KIST), Seoul 02792, Republic of Korea

^dRobert F. Smith School for Chemical and Biomedical Engineering, Cornell University, Ithaca, NY 14850, United States

ABSTRACT: Hydrogen sulfide (H₂S) is an endogenously produced gasotransmitter involved in many physiological processes that are integral to proper cellular functioning. Due to its profound anti-inflammatory and antioxidant properties, H₂S plays important roles in preventing inflammatory skin disorders and improving wound healing. Transdermal H₂S delivery is a therapeutically viable option for the management of such disorders. However, current small-molecule H₂S donors are not optimally suited for transdermal delivery and typically generate electrophilic byproducts that may lead to undesired toxicity. Here, we demonstrate that H₂S release from metal-organic frameworks (MOFs) bearing coordinatively unsaturated metal centers is a promising alternative for controlled transdermal delivery of H₂S. Gas sorption measurements and powder X-ray diffraction (PXRD) studies of eleven MOFs support that the Mg-based framework Mg₂(dobdc) (dobdc⁴⁻ = 2,5-dioxidoobenzene-1,4-dicarboxylate) is uniquely well-suited for transdermal H₂S delivery due to its strong yet reversible binding of H₂S, high capacity (14.7 mmol/g at 1 bar and 25 °C), and lack of toxicity. In addition, Rietveld refinement of synchrotron PXRD data from H₂S-dosed Mg₂(dobdc) supports that the high H₂S capacity of this framework arises due to the presence of three distinct binding sites. Last, we demonstrate that transdermal delivery of H₂S from Mg₂(dobdc) is sustained over a 24 h period through porcine skin. Not only is this significantly longer than sodium sulfide, but this represents the first example of controlled transdermal delivery of pure H₂S gas. Overall, H₂S-loaded Mg₂(dobdc) is an easily accessible, solid-state source of H₂S, enabling safe storage and transdermal delivery of this therapeutically relevant gas.

INTRODUCTION

Since the discovery of endogenously produced hydrogen sulfide (H₂S) in living tissues,^{1,2} this toxic, flammable gas has been identified as the third gasotransmitter, joining nitric oxide (NO) and carbon monoxide (CO).³ Within humans, H₂S is important for maintaining normal physiological functions, as it mitigates inflammation, promotes angiogenesis, and attenuates oxidative stress arising from high levels of reactive oxygen species and related cellular injuries.^{4,5} Consequently, H₂S has been investigated as a therapeutic agent for various diseases and disorders, such as hypertension, Alzheimer's disease, ischemia-reperfusion injury, atherosclerosis, and diabetes.⁶⁻⁸ In addition, H₂S has recently been implicated for the treatment of many skin pathologies and cancers.⁹ Abnormally low H₂S levels in skin tissues have been linked to inflammatory disorders, such as psoriasis, as well as to chronic wounds and skin ulcers.^{6,10} As such, reliable methods for transdermal H₂S delivery offer the potential for treating these and other skin-related disorders.

Transdermal delivery of gaseous H₂S via small-molecule donors such as sodium sulfide (Na₂S) and sodium hydrosulfide (NaSH) remains the most attractive current method of administration.^{11,12} In addition, incorporation of H₂S prodrugs into various gels, mats, or fibrous polymers as wound dressings has been shown to improve the consistency of H₂S release and offer wound protection.¹³⁻²⁰ However, depending on the method of H₂S release, many of these small molecules suffer from limited stability and undesirable side effects that arise from electrophilic byproducts.^{21,22} In addition, the rapid H₂S release from these donors, especially inorganic sulfide salts, could potentially lead to a high concentration of the gas accumulating at the site of delivery, resulting in local cell death (Fig. 1, left).^{19,21,23} Use of Na₂S and NaSH in particular often presents difficulties with ensuring consistent dosing due to some volatilization of H₂S post-delivery.^{24,25} For example, previous *in vitro* studies investigating the effects of exogenous NaSH supplementation on human keratinocytes observed cell proliferation to be highly dose-

Inorganic sulfide salts

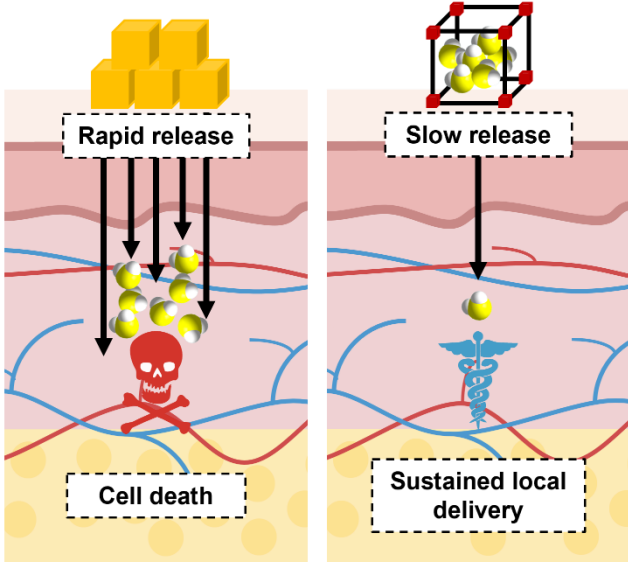


Figure 1. Transdermal H₂S delivery using common inorganic sulfide-containing salts such as Na₂S suffer from rapid H₂S release upon skin contact leading to a high H₂S concentration, resulting in cell death (left). By contrast, slow H₂S release from porous materials such as MOFs may result in improved sustained local H₂S delivery at therapeutic concentrations (right).

dependent; while low (<1 mM) concentrations enhanced cell differentiation,²⁶ higher (>1 mM) concentrations instead promoted apoptotic activity.²⁷ Additional related work found that only intradermal injections of Na₂S or NaSH elicited itch sensations in mice, whereas an identical dosage of the slow-release H₂S donor GYY4137 did not result in the same physiological effect, suggesting that rapid H₂S release may be associated with inflammatory-like responses.²⁸ An *in vitro* study directly comparing NaSH and GYY4137 on the release of either pro- or anti-inflammatory mediators in macrophages corroborated this finding; only GYY4137 consistently inhibited cytokine production, whereas NaSH either increased inflammatory markers or gave inconsistent results at lower concentrations.²⁹ These studies highlight the careful control needed not only over the concentration of H₂S but also over the rate at which it is delivered to avoid potential toxicity and mimic endogenous H₂S production rates.

As an alternative to small-molecule donors, we propose that gaseous H₂S itself can be loaded into porous materials such as metal-organic frameworks (MOFs), providing a promising alternative to traditional H₂S-based therapeutics (Fig. 1, right).³⁰ The structural tunability of MOFs makes them attractive drug delivery systems (DDS) for active pharmaceutical ingredients (APIs), including common drugs, cosmetics, and gasotransmitters.^{31–34} The transdermal delivery route offers several advantages over other modes of administration for MOF-based DDS. For example, drug-loaded MOFs injected directly into the bloodstream must be within a certain particle size range, typically 10–200 nm, to avoid rapid kidney clearance or immune system destruction,

effectively limiting the amount of active API reaching the target of interest if the MOF is removed from circulation too quickly.³⁵ Because the MOF itself is unlikely to pass through the skin, this limitation is avoided in subcutaneous delivery. Furthermore, transdermal delivery avoids the harshly acidic environment of the stomach encountered in oral drug administration, which would typically cause MOF degradation and instant cargo release. Transdermal MOF-based DDS have already proved promising for the subcutaneous delivery of drugs such as salicylic acid, ibuprofen, ferulic acid, and caffeine.^{36–40} However, drug release profiles from these systems are characterized by a “burst” phase followed by more gradual release of the remaining drug. This is a commonly observed phenomenon in other heterogeneous DDS and is often considered a drawback in systems designed with slow release in mind.⁴¹ In addition, the potential side effects of the framework on epidermal and dermal cells have not been thoroughly addressed, though one study reported good biocompatibility between the MOF and dermal fibroblasts.⁴⁰ Likewise, although MOF-based DDS have been designed for NO^{42–44} and CO,^{45–47} there have been comparatively few such systems tailored for H₂S delivery.^{30,48} Its inherent reactivity and incompatibility with many materials makes constructing a porous material capable of storing and releasing H₂S a major challenge.^{49,50}

Recently, we have shown that the biocompatible Zr-based MOF, Zr-fum (fum = fumarate) or MOF-801, is capable of reversibly binding H₂S via hydrogen-bonding interactions between the gas and nodes of the framework.³⁰ Through triggered release upon exposure to aqueous solution, Zr-fum was able to deliver H₂S to injured cells in an *in vitro* hypoxia-reoxygenation model that simulates ischemia-reperfusion injury. Despite these promising results, Zr-fum rapidly loses H₂S in air, making it unsuitable for transdermal delivery. Gradual, sustained H₂S release is crucial not only to prevent potential cytotoxicity caused by a sudden surge in localized H₂S concentration, but also to mimic endogenous H₂S production rates.⁵¹ We hypothesized that strengthening the interaction between H₂S and the porous framework would lead to slower release under ambient conditions. Because H₂S is Lewis basic, selecting a framework with accessible Lewis acidic sites should result in a much stronger interaction and thus slower H₂S release.⁵² For example, MOFs bearing open metal sites or coordinatively unsaturated metal centers represent a diverse class of materials extensively studied for their ability to strongly bind guest molecules through Lewis acid-base interactions.⁵³ However, their suitability for binding H₂S remains largely unstudied. In addition, there are numerous reports concerning the degradation of MOFs by H₂S, representing an additional challenge.⁵⁴

Herein, we evaluate eleven frameworks from three well-known families of open metal site MOFs for their promise as transdermal H₂S donors. Through gas sorption and cytotoxicity measurements, we demonstrate that only one framework—Mg₂(dobdc) (dobdc⁴⁻ = 2,5-dioxidobenzene-1,4-dicarboxylate)—exhibits strong, reversible, and high-capacity binding of H₂S coupled with good biocompatibility.

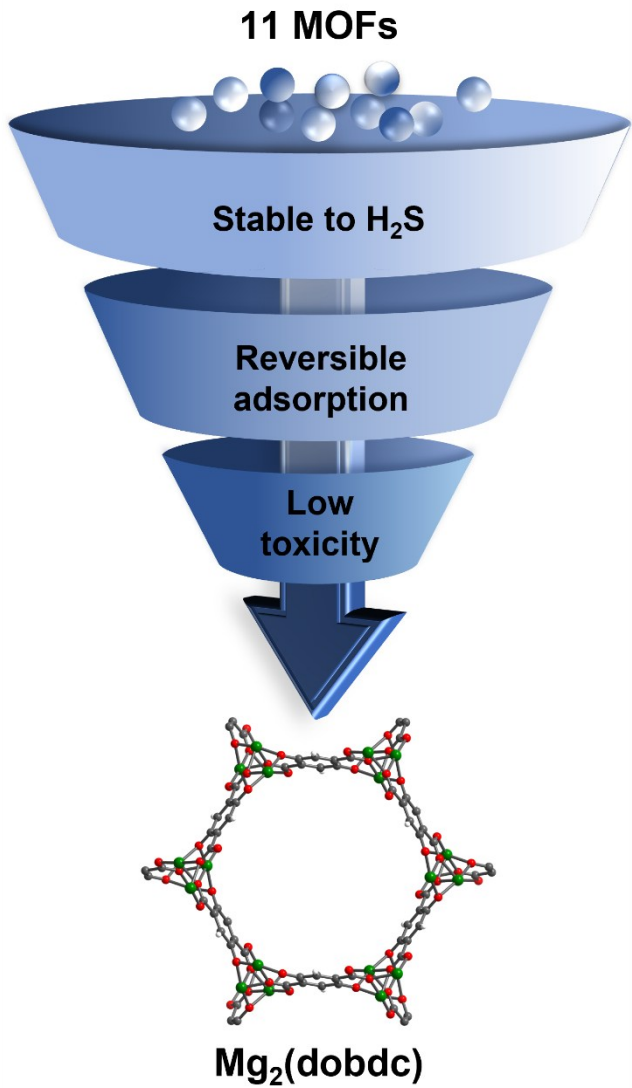


Figure 2. Criteria for the systematic evaluation of eleven open metal site MOFs to determine their suitability for transdermal H₂S delivery, leading to Mg₂(dobdc) as the optimal material.

Structural characterization via synchrotron powder X-ray diffraction (PXRD) reveals three distinct binding sites of H₂S in the hexagonal channels of the framework, accounting for its very high H₂S capacity (14.7 mmol/g or 33.3 wt% at 1 bar and 25 °C). Using a Franz cell apparatus, we demonstrate that H₂S-loaded Mg₂(dobdc) can sustain H₂S release through porcine skin under ambient conditions over a period of 24 h, significantly longer than a Na₂S control. Taken together, our findings suggest that loading gaseous H₂S into Mg₂(dobdc) represents a promising new avenue for the gradual transdermal delivery of this therapeutically underutilized gas.

RESULTS & DISCUSSION

Although H₂S adsorption has been studied in a range of MOFs,^{54–62} mostly in the context of H₂S removal from contaminated gas streams, the majority of these frameworks

are not suitable for therapeutic transdermal delivery. This limitation is a consequence of the presence of toxic or air-sensitive metal centers, such as in the case of MIL-53(Cr),⁶³ as well as their relatively weak interaction with H₂S, leading to its rapid loss upon exposure to air.⁵⁶ For example, many MOFs reported to reversibly bind H₂S exhibit enthalpies of adsorption ($-H_{ads}$) for H₂S of less than 30 kJ/mol (see supporting information or SI Table S7), including MIL-53(Al)-TDC, the MOF with the highest reported H₂S capacity to date.⁶⁴ In search of potentially biocompatible materials that also strongly bind H₂S, we turned to the canonical M₂(dobdc) or MOF-74 family of materials. These frameworks feature rigid one-dimensional hexagonal channels decorated with coordinately unsaturated M²⁺ sites.^{65–67} In addition, the Mg variant has previously been used as a drug delivery vehicle.⁶⁸ The related isomeric M₂(*m*-dobdc) (*m*-dobdc⁴⁻ = 2,4-dioxidobenzene-1,3-dicarboxylate) family of frameworks possesses an even higher volumetric density of M²⁺ sites capable of interacting strongly with gases such as H₂ and CO₂.^{69,70} In addition to the aforementioned materials, the azolate frameworks M₂Cl₂(btdd) (btdd²⁻ = bis(1,2,3-triazolo[4,5-*b*],[4',5'-*i*]dibenz[1,4]dioxin)⁷¹ and Ni₃(ntp)₂ (ntp³⁻ = 4,4',4''-(benzene-1,3,5-trityl)tris(pyrazolate))⁷² were selected for study due to their potentially enhanced stability towards H₂S. M₂Cl₂btdd MOFs feature an analogous topology to M₂(dobdc) but are more robust due to the higher basicity of their triazolate linkers.⁷¹ Similarly, the high basicity of the pyrazolate linker in Ni₃(ntp)₂, a framework possessing accessible square planar Ni²⁺ sites, lends it excellent hydrolytic stability.⁷³

Based on these criteria, eleven open metal site MOFs were prepared following literature procedures: M₂(dobdc) (M = Mg, Ni, Zn, Cu, Co), M₂(*m*-dobdc) (M = Mg, Ni, Co), M₂Cl₂(btdd) (M = Ni, Co), and Ni₃(ntp)₂ (see SI section 2 for details). The successful synthesis and activation of all MOFs were confirmed by PXRD and 77 K N₂ surface area measurements (SI section 2). In order to systematically narrow down these frameworks for H₂S transdermal delivery, they were evaluated based on three key criteria (Fig. 2): (1) the stability of the MOF towards H₂S in solution, (2) the ability of the MOF to reversibly adsorb gaseous H₂S, and (3) the minimal cytotoxicity of the MOF towards human cell lines. First, assessing the stability of frameworks to a solution of H₂S eliminates MOFs that do not retain crystallinity from contention.⁷³ Pawley refinement of the resulting PXRD pattern allows for further quantification of crystallinity by taking into account the change in the volume weighted average crystalline domain size (LVol-IB) upon H₂S exposure. This additional characterization is crucial to ascertain whether partial dissolution or framework modification may have taken place upon H₂S exposure.^{73,74} Second, H₂S adsorption isotherms of frameworks that do retain crystallinity upon exposure to a solution of H₂S allow for the measurement of H₂S sorption properties including reversibility, capacity, and binding strength. Importantly, evaluation of porosity before and after gaseous H₂S exposure ensures fully reversible binding as well as a lack of potential byproducts such as

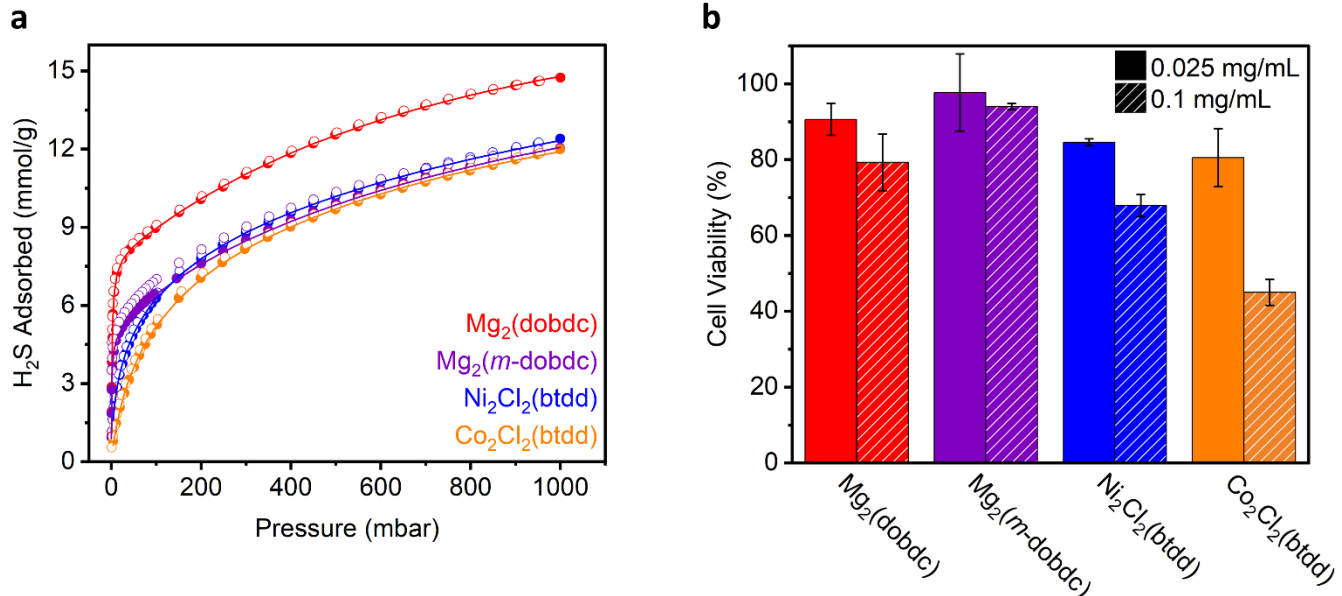


Figure 3. (a) H₂S adsorption (closed circles) and desorption (open circles) isotherms at 25 °C for activated Mg₂(dobdc) (red), Mg₂(m-dobdc) (purple), Ni₂Cl₂(btdd) (blue), and Co₂Cl₂(btdd) (orange). Solid lines represent simultaneous fits of the adsorption data to a Langmuir-Freudlich model. A data point was considered equilibrated after <0.01% pressure change occurred over a 45 s interval. (b) Viability of HeLa cells upon exposure to suspensions of Mg₂(dobdc) (red), Mg₂(m-dobdc) (purple), Ni₂Cl₂(btdd) (blue), or Co₂Cl₂(btdd) (orange) at concentrations of 0.025 mg/mL (solid) or 0.1 mg/mL (striped) in DMEM supplemented with 10% FBS at 37 °C. Viabilities were determined by incubating the cells with MTT followed by colorimetric analysis using a microplate reader. Results are reported as the average cell viability of 6 wells/concentration compared to untreated cells from three independent trials, with the standard deviation (SD) reported as the error (±SD).

metal sulfides.⁶³ Last, for these MOFs to be suitable for biomedical applications, they must be nontoxic. *In vitro* cytotoxicity measurements provide a facile means of assessing the potential off-target side effects that may occur when these MOFs are used for transdermal delivery.

In order to quickly eliminate frameworks that are not stable towards H₂S, freshly activated MOFs were submerged in a commercially available solution of H₂S in tetrahydrofuran (THF) under N₂ at 50 °C for 24 h (SI section 3). After this time, any remaining solid was filtered, rinsed with additional THF, and characterized by PXRD to confirm the robustness of the MOF towards H₂S.⁷³ Upon addition of the H₂S solution, Cu₂(dobdc), Co₂(dobdc), Co₂(m-dobdc), and Zn₂(dobdc) immediately turned black. After 24 h, no solid could be isolated for these four materials. This observation is consistent with the poor H₂S stability of the Cu and Zn-based MOFs HKUST-1 and MOF-5,⁵⁵ respectively, as well as previous findings that Zn₂(dobdc) is not stable towards gaseous H₂S.^{30,48} As a strong nucleophile, H₂S likely displaces linkers on the metal nodes, leading to the formation of metal sulfide species. Uniquely among Co-based MOFs, Co₂Cl₂(btdd) appeared to remain crystalline upon visual inspection of the powder pattern after exposure to H₂S solution (SI Fig. S54). The strong metal-nitrogen bonds in this framework likely impart better kinetic stability towards metal sulfide formation.⁷⁵ It is important to note, however, that the LVol-IB value calculated from Pawley refinement of the post-H₂S pattern substantially decreased from that of the pristine MOF, suggesting that there may have been some

framework dissolution upon H₂S exposure (SI Fig. S55 and S56). Notably, all tested Mg-based (Mg₂(dobdc), Mg₂(m-dobdc)) and Ni-based (Ni₂(dobdc), Ni₂(m-dobdc), Ni₂Cl₂(btdd), Ni₃(btpp)₂) frameworks exhibited minimal changes by PXRD upon prolonged exposure to H₂S in solution (SI Fig. S41, S44, S48, S51, S57, and S60).

H₂S adsorption/desorption isotherms were next measured at 25 °C for the seven MOFs that were found to be stable towards H₂S in solution (Fig. 3a, SI section 4). H₂S uptake at 25 °C proved irreversible at low pressures (<50 mbar) for Ni-based MOFs Ni₂(dobdc), Ni₂(m-dobdc), and Ni₃(btpp)₂, as indicated by the lack of complete desorption in the H₂S isotherms (SI Fig. S70, S84, and S105, respectively). The Brunauer-Emmett-Teller (BET) surface areas of Ni₂(dobdc) and Ni₂(m-dobdc) were found to decrease by 36% and 33%, respectively, after the H₂S sorption isotherms, even with reactivation at 180 °C or 200 °C under high vacuum (10 μbar) (SI Fig. S71 and S85). In addition, X-ray photoelectron spectroscopy (XPS) analysis of Ni₂(dobdc) and Ni₂(m-dobdc) after the H₂S isotherms revealed the presence of sulfur-containing species in the high-resolution S2p spectral region, even after extensive evacuation (SI Fig. S77 and S91). It is highly likely from the broad spectral features in this region that multiple sulfur species are present, including polysulfides as well as metal sulfides and sulfates.⁷⁶ Rather than just H₂S adsorption on the open Ni²⁺ sites, it is likely that further reactions are taking place inside the pores. Thermo-gravimetric analysis (TGA) supports this hypothesis, as an expected weight loss attributable to H₂S desorbing from the

pores of both frameworks was not observed upon heating up to 600 °C (SI Fig. S75 and S89). Furthermore, both materials exhibited a color change from green to black upon H₂S uptake, indicative of a chemical reaction taking place. The Ni-based MOF Ni₃(btp)₂ similarly exhibited a 26% reduction in BET surface area after exposure to gaseous H₂S (SI Fig. S106). Despite this partial loss in porosity due to irreversible H₂S uptake, all three materials retained crystallinity by PXRD, indicating that H₂S exposure does not lead to complete amorphization or to new crystalline phases (SI Fig. S76, S90, and S108). As such, irreversible H₂S uptake (along with Ni allergies being well-established in many people)⁷⁷ make these three frameworks unsuitable for transdermal delivery. These findings underline the importance of measuring N₂ uptake before and after H₂S sorption measurements to establish the complete reversibility of H₂S binding in a given material, as retention of crystallinity alone is not enough to establish that a MOF is stable towards H₂S.^{48,78}

The four remaining frameworks, Mg₂(dobdc), Mg₂(*m*-dobdc), Co₂Cl₂(btdd), and Ni₂Cl₂(btdd), display fully reversible H₂S adsorption at 25 °C (Fig. 3a). With the exception of Co₂Cl₂(btdd), no evidence of H₂S-mediated decomposition was observed for any of these materials, as all retained full crystallinity (SI Fig. S67, S82, and S103) and porosity (SI Fig. S65, S80, and S101) after H₂S adsorption/desorption measurements. Similar to the results obtained from solution-state H₂S exposure, Co₂Cl₂(btdd) exhibited a substantial loss in crystallite size after gaseous H₂S exposure, indicating some damage to the framework (SI Fig. S96 and S97); however, no corresponding change in surface area was observed (SI Fig. S94).

To investigate any H₂S-mediated morphological changes, scanning electron microscopy (SEM) images were collected of all four frameworks before and after exposure to gaseous H₂S. SEM images of H₂S-exposed Co₂Cl₂(btdd) revealed marked surface roughness not initially present as well as an overall decrease in average crystallite size compared to the as-synthesized MOF (SI Fig. S98), corroborating the conclusions drawn from Pawley refinement of the PXRD data. While Ni₂Cl₂(btdd) exhibited no such decrease in crystallinity by PXRD, some crystallite destruction was likewise observed by SEM (SI Fig. S104), highlighting the need for both techniques to accurately assess framework integrity towards H₂S. Unlike the azolate frameworks, both Mg₂(dobdc) and Mg₂(*m*-dobdc) retained their needle-like morphology and uniform crystallite size before and after H₂S exposure (SI Fig. S69 and S83).

In addition to the above morphological changes, crucial differences in H₂S sorption properties were observed among the four frameworks. The low-pressure region (<50 mbar) of the isotherms is appreciably steeper for Mg₂(dobdc) and Mg₂(*m*-dobdc) than for Co₂Cl₂(btdd) and Ni₂Cl₂(btdd), indicating that H₂S binds more strongly in the former two frameworks (see discussion below). This is likely because the stronger field ligands in the azolate-based M₂Cl₂(btdd) MOFs reduce the Lewis acidity of the metal centers. In

addition, Mg₂(dobdc) possesses by far the highest H₂S capacity (14.7 mmol/g or 33.3 wt% at 1 bar and 25 °C) among the four MOFs. With such a high potential deliverable capacity, Mg₂(dobdc) concentrations as low as 0.01 mg/mL could deliver H₂S at μM-level therapeutic doses.^{79,80} This capacity is among the highest reported to date for a MOF under these conditions, surpassed only by MIL-53(Al)-TDC (18.1 mmol/g).⁶⁴ Although Mg₂(*m*-dobdc) should theoretically possess a similar capacity to Mg₂(dobdc), its maximum H₂S uptake at 1 bar is only 12.0 mmol/g. This lower capacity is consistent with its lower BET surface area (1515 m²/g) compared to Mg₂(dobdc) (1800 m²/g). Ni₂Cl₂(btdd) and Co₂Cl₂(btdd) exhibit similar capacities to each other under the same conditions (12.4 and 12.0 mmol/g, respectively).

We next evaluated the toxicity of all four materials to determine whether Mg₂(dobdc) is truly the most suitable framework for transdermal H₂S delivery (Fig. 3b, SI section 5). Briefly, HeLa cells were exposed to varying concentrations of the MOFs suspended in Dulbecco's Modified Eagle's Medium (DMEM) supplemented with 10% fetal bovine serum (FBS) for 72 h at 37 °C. To determine viability, cells were then incubated with (4,5-dimethylthiazol-2-yl)-2,5-diphenyltetrazolium bromide (MTT) followed by colorimetric quantification.⁸¹ This was compared to quantification of cells not exposed to the MOF suspension (defined as 100% viability). Mg₂(dobdc) is effectively nontoxic (>90% viability) at concentrations below 0.1 mg/mL, with viabilities dipping to around 80% at this concentration. Additional cytotoxicity measurements using an immortalized keratinocyte cell line (HaCaT) more relevant to transdermal drug delivery are within 10% of HeLa cell viabilities at concentrations below 0.1 mg/mL (SI Fig. S113). At all concentrations up to 0.1 mg/mL, Mg₂(*m*-dobdc) also demonstrates excellent compatibility with HeLa cells (Fig. 3b). Both salicylate frameworks are less toxic than Ni₂Cl₂(btdd) and Co₂Cl₂(btdd), further ruling out these two materials as suitable for H₂S delivery. Although the two salicylate frameworks exhibit similarly steep H₂S adsorption properties and minimal toxicities, the higher deliverable capacity of Mg₂(dobdc) makes it the most promising material to evaluate further for transdermal H₂S delivery.

To understand the origin of strong H₂S binding in Mg₂(dobdc), 40 °C and 55 °C H₂S adsorption/desorption isotherms for this material were collected in addition to the 25 °C isotherm (Fig. 4a). For comparison, the same isotherms were collected for Mg₂(*m*-dobdc), Ni₂Cl₂(btdd), and Co₂Cl₂(btdd) as well (SI section 4). The isotherms were fit simultaneously to dual-site Langmuir-Freundlich models to enable calculation of the differential enthalpies of H₂S adsorption ($-\Delta H_{ads}$) as a function of H₂S loading (Fig. 4b). Two distinct binding regimes were observed. At low H₂S loadings, adsorption presumably occurs at the vacant Mg²⁺ sites, with a relatively favorable $-\Delta H_{ads}$ of 42.97 ± 0.01 kJ/mol. Once these primary binding sites are saturated, additional adsorption occurs at weaker secondary binding sites, as evidenced by a sharp dip followed by a plateau at a $-\Delta H_{ads}$ of

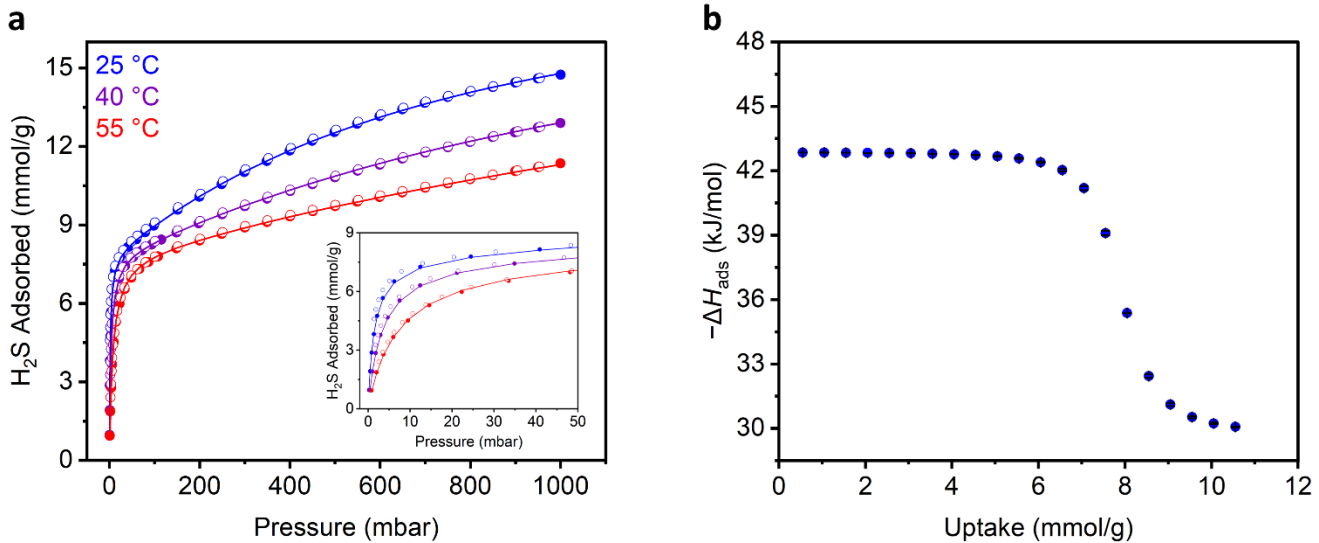


Figure 4. (a) H₂S adsorption (closed circles) and desorption (open circles) isotherms at 25 °C (blue), 40 °C (purple), and 55 °C (red) of activated Mg₂(dobdc). Solid lines represent simultaneous fits of the adsorption data to a Langmuir-Freundlich model. A data point was considered equilibrated after <0.01% pressure change occurred over a 45 s interval. Inset: Low-pressure region up to 50 mbar of the H₂S adsorption isotherm in panel (a). (b) Differential enthalpies of adsorption ($-\Delta H_{ads}$) for H₂S as a function of uptake for activated Mg₂(dobdc) as determined by using the Clausius-Clapeyron equation (eqn. (S1)) and Langmuir-Freundlich fits in panel (a). Error bars for each data point are too small to see.

30.60 ± 0.04 kJ/mol. The loading at which this transition occurs (~ 7 mmol/g) is close to the theoretical loading of 8.4 mmol/g assuming one H₂S molecule per Mg²⁺ site. Similar behavior was observed in Mg₂(*m*-dobdc) (SI Fig. S79). Although H₂S adsorption is about 10 kJ/mol stronger at low loadings in this framework (53 kJ/mol vs 43 kJ/mol), the characteristic transition from primary to secondary adsorption sites occurs at lower loadings (4.5 mmol/g) likely due to fewer accessible Mg²⁺ sites, leading to an overall lower H₂S capacity. In contrast, H₂S binding in Co₂Cl₂(btdd) and Ni₂Cl₂(btdd) becomes significantly less favorable as a function of uptake (SI Fig. S93 and S100), accounting for the shallow adsorption isotherms of these two materials (Fig. 3a).

The preferred H₂S binding mode(s) in Mg₂(dobdc) were probed by synchrotron PXRD collected on H₂S-dosed micro-crystalline Mg₂(dobdc) (Fig. 5) and by density functional theory (DFT) calculations (SI section 9). Rietveld refinement of the PXRD pattern of H₂S-Mg₂(dobdc) supports that the primary site of H₂S binding is at the open Mg²⁺ site, with a S···Mg interaction distance of 2.344(19) Å (site I, Fig. 5a). This short distance is consistent with reported magnesium complexes containing thiol or thiolate ligands, which have S···Mg bond distances of 2.3–2.4 Å (SI Table S5).^{82–86} The few reported complexes in which either H₂S or SH⁻ is directly bound to a metal center, including Mn,⁸⁷ Os,⁸⁸ and Ru^{89–92} complexes, also possess comparable metal-sulfur bond distances of 2.33–2.45 Å (SI Table S6). The interaction between H₂S and the Mg²⁺ site in Mg₂(dobdc) is on the shorter side of this range likely due to the small size of the Mg²⁺ cation. Further supporting this short interaction distance, previous structures of water bound in M₂(dobdc) frameworks contain even shorter metal-OH₂ distances (2.1–2.15 Å),^{93,94}

with an O···Mg interaction in water-bound Mg₂(dobdc) of 2.0892(15) Å.⁹⁵ Additional H₂S molecules in the secondary binding site are oriented towards those bound to the primary site through S–S interactions, with a S···S distance of 2.504(12) Å (site II, Fig. 5a). Previous studies on H₂S dimers report a much longer S···S distance of 4.112(1) Å,⁹⁶ suggesting that the interaction between H₂S molecules in binding sites I and II in the MOF is more covalent in nature. The strongly polarized Mg–S interaction likely results in a buildup of partial positive charge on the H₂S molecule in binding site I, inducing enhanced interaction with H₂S molecules in binding site II. Consistently, S–S bonds found in polysulfide and disulfide species are even shorter; for example, a typical disulfide bond is around 2.05 Å in length.⁹⁷ A DFT-calculated model further supports the presence of the two major H₂S binding sites I and II in Mg₂(dobdc), albeit with slightly longer Mg–S and S–S bond lengths (SI Fig. S139). The calculated binding energies ($-E_b$) of H₂S in sites I (53.5 kJ/mol) and II (32.5 kJ/mol) match well with experimentally obtained $-\Delta H_{ads}$ values (43.0 and 30.6 kJ/mol, respectively). A third binding site in the center of the pore could also be resolved, contributing to the high H₂S capacity of this material (site III, Fig. 5a).

Further evidence for strong H₂S binding in Mg₂(dobdc) was obtained using diffuse reflectance infrared Fourier transform spectroscopy (DRIFTS) (SI section 12). The IR spectrum of H₂S-dosed Mg₂(dobdc) reveals a new broad stretch not present in the activated MOF in the 2400–2600 cm⁻¹ range, which can be attributed to H₂S bound in the framework (SI Fig. S142).^{62,78} Under flowing N₂, this peak was observed to decrease in intensity and slightly red-shift, likely due to loss of weakly bound H₂S at secondary binding sites (II, III, Fig. 5). However, this peak remained in the DRIFTS

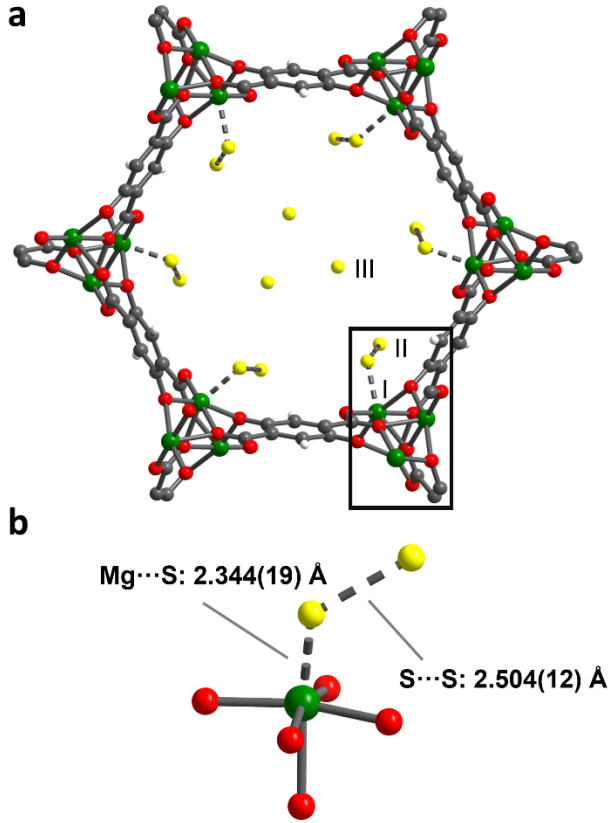


Figure 5. (a) Structural model of $\text{Mg}_2(\text{dobdc})$ dosed with 10 mbar of H_2S obtained from Rietveld refinement of synchrotron PXRD data. Primary, secondary, and tertiary adsorption sites are indicated by I, II, and III, respectively. Occupancies for sites I, II, and III, are 0.7676, 0.9201, and 0.9558, respectively. Hydrogen atoms on H_2S molecules were not resolved. (b) Coordination environment of one Mg^{2+} metal site in panel (a) highlighting sites I and II of H_2S adsorption as well as key bond lengths. Gray, white, red, green, and yellow spheres correspond to carbon, hydrogen, oxygen, magnesium, and sulfur, respectively.

spectrum after 24 h under flowing N_2 , suggesting that N_2 cannot displace H_2S bound to the open Mg^{2+} sites (I, Fig. 5). In contrast, flowing N_2 over H_2S -dosed Zr-fum resulted in the disappearance of the characteristic stretch at 2500–2600 cm^{-1} within 10 min, indicative of much weaker H_2S binding in this framework (SI Fig. S143). Overall, these data support the presence of a strongly polarizing interaction of H_2S with Lewis acidic Mg^{2+} sites, which accounts for a significantly higher H_2S capacity of $\text{Mg}_2(\text{dobdc})$ compared to most studied materials developed for transdermal delivery.

Having established that $\text{Mg}_2(\text{dobdc})$ strongly and reversibly adsorbs H_2S and is nontoxic to human cells at therapeutic concentrations, we explored whether alternative stimuli to vacuum could trigger H_2S desorption from $\text{Mg}_2(\text{dobdc})$ under more biologically relevant conditions. Given the strong binding of water in open metal site MOFs,⁹⁸ it is likely that water is capable of facilitating H_2S release from the framework. To test this hypothesis, a known amount of H_2S -dosed

$\text{Mg}_2(\text{dobdc})$ was suspended in a stirring solution of HEPES buffer (pH 7.4) (SI section 6). From this mixture, aliquots were removed at designated time points and analyzed with the fluorescence probe sulfidefluor-7 acetoxymethyl ester (SF7-AM), which exhibits turn-on fluorescence ($\lambda_{\text{max}} = 525 \text{ nm}$) upon irreversible reaction with H_2S .⁹⁹ The release of H_2S from $\text{Mg}_2(\text{dobdc})$ was monitored over time via fluorescence spectroscopy. Upon incubation in this buffer, the concentration of H_2S in solution gradually saturated over a period of 10–20 min and was maintained over 30 min (SI Fig. S118 and S119). Notably, the release rate of H_2S from $\text{Mg}_2(\text{dobdc})$ is slower than that from Zr-fum.³⁰ When H_2S -loaded Zr-fum was suspended in HEPES buffer, peak H_2S concentration in solution was reached rapidly, within only 1 to 2 min, and these levels were maintained for only 10 min (SI Fig. S116 and S117). These results are consistent with the stronger H_2S binding of $\text{Mg}_2(\text{dobdc})$ compared to Zr-fum (43 kJ/mol vs. 32 kJ/mol, respectively).³⁰ This process was concomitant with the conversion of the suspension to a homogeneous solution over the course of 1 h (SI Fig. S122). In addition, UV-Vis spectroscopic monitoring of a suspension of $\text{Mg}_2(\text{dobdc})$ in HEPES buffer revealed a gradual formation of an absorbance band at 351 nm, a feature characteristic of free linker presence in solution (SI section 7 and SI Fig. S121). The stability of the $\text{M}_2(\text{dobdc})$ family to aqueous conditions has previously been explored,^{100,101} and it is known that the dobdc^{4-} linker is prone to protonation resulting in framework dissolution.⁷³ Nonetheless, depending on the pharmacological mode of administration, such as transdermal delivery, the gradual dissolution of $\text{Mg}_2(\text{dobdc})$ in aqueous media could act as a natural means of self-clearance from the body after H_2S delivery, rather than a drawback.

This MOF was next investigated as a transdermal delivery agent for the treatment of diseases of the skin (Fig. 6). To this end, an *ex vivo* Franz cell model was used (SI section 8).^{11,40} Porcine skin was chosen as a surrogate for human skin due to its similar histological and physiological markers, thickness, and anatomy.^{102,103} The porcine dermal samples were collected posthumously and applied as a membrane between the two chambers of the Franz cell. A known amount of H_2S -loaded $\text{Mg}_2(\text{dobdc})$ was packed into the top donor chamber while HEPES buffer (pH 7.4) was added to the bottom acceptor chamber (SI Fig. S127). At designated time points, aliquots were removed from the side arm of the acceptor chamber and quenched with SF7-AM solution. A small amount (20 μL) of HEPES buffer was then added to the MOF to facilitate H_2S diffusion from the MOF to skin. The concentration of H_2S in the acceptor chamber was observed to increase slowly over a period of 24 h up to a maximum of between 3 and 6 mM, at which point it began to decrease, likely due to leakage from the Franz cell (Fig. 6, SI Fig. S128, S130, S132). The rate of transdermal H_2S release can be estimated based on the approximate linear increase as 5 μM $\text{H}_2\text{S}/\text{mg MOF}/\text{h}$ (SI Fig. S129, S131, S133), well within the therapeutic window with just 5–10 mg of MOF.^{104–106} Crucially, a control experiment in which an equivalent amount of Na_2S was packed in the donor chamber instead of the

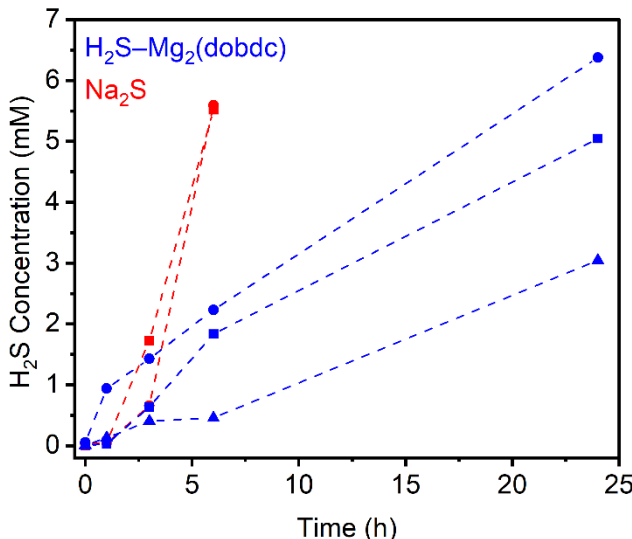


Figure 6. Transdermal H₂S release from Mg₂(dobdc) (blue) and Na₂S (red) through porcine skin detected with SF7-AM via fluorescence spectroscopy over time. Each dotted line with a corresponding shape represents a different trial. H₂S released from Mg₂(dobdc) increases linearly until reaching a maximum at 24 h. By contrast, Na₂S delivers H₂S much more rapidly with the maximum H₂S concentration detected within 6 h.

MOF resulted in much more rapid H₂S release, with peak concentrations reached in only 6 h before declining (Fig. 6, SI Fig. S134 and S136). The significantly slower rate of delivery from H₂S-loaded Mg₂(dobdc) is crucial to the successful healing of wounds and other inflammatory skin conditions,²² indicating that that this materials is a much more promising H₂S transdermal delivery agent compared to Na₂S alone.

CONCLUSIONS

Transdermal delivery of H₂S for the treatment of topical wounds and skin diseases and disorders remains a challenge, due to both the hazards of working with gaseous H₂S and the innate difficulty in designing a suitable storage and delivery platform for it. Here, by systematically evaluating the H₂S sorption characteristics and cytotoxicities of eleven open metal site MOFs, we demonstrate that Mg₂(dobdc) is the best for transdermal H₂S delivery. It is clear from these assays that the redox inert Mg²⁺ center in Mg₂(dobdc) facilitates strong H₂S uptake while preventing framework decomposition due to metal sulfide formation. In contrast, H₂S uptake in all tested transition metal-based frameworks is either weak (M₂Cl₂(btdd), M = Co, Ni) or results in (partial) framework destruction (all others). Thus, our findings have important implications for the design of next-generation materials for H₂S capture and delivery.

The outstanding H₂S capacity and binding strength in Mg₂(dobdc) coupled with its nontoxic nature and relative stability in air result in slow transdermal release of H₂S sustained for at least 24 h, significantly longer than an equivalent amount of Na₂S. Future work will focus on integration

of the framework into patches or membranes to improve handleability and processability for cutaneous application on animal model systems.

ASSOCIATED CONTENT

Supporting Information

The Supporting Information is available free of charge at <http://pubs.acs.org>.

Synthetic, computational, and crystallographic protocols, as well as all other procedures and data (PDF)

Experimental crystal data for H₂S in Mg₂(dobdc) (CCDC 2325508) (CIF)

Accession Codes

CCDC 2325508 contains the supplementary crystallographic data for this paper. These data can be obtained free of charge via www.ccdc.cam.ac.uk/data_request/cif, or by emailing data_request@ccdc.cam.ac.uk, or by contacting The Cambridge Crystallographic Data Centre, 12 Union Road, Cambridge CB2 1EZ, UK; fax: +44 1223 336033.

AUTHOR INFORMATION

Corresponding Author

* pjm347@cornell.edu

Present Addresses

† Chemical Sciences Division, Lawrence Berkeley National Laboratory, Berkeley, California 94720, United States

Author Contributions

‡ R.M.M. and P.S.L. contributed equally to this work. P.J.M. and J.J. Wilson conceived the project. R.M.M. synthesized and characterized all MOFs and carried out all H₂S adsorption measurements. P.S.L. carried out all transdermal and solution-state H₂S delivery experiments. T.R. refined the structure of H₂S in Mg₂(dobdc). J.L. carried out DFT calculations. J.J.W. carried out cytotoxicity measurements. T.A.P. conducted Pawley refinements for solution-state H₂S stability assays. The manuscript was written through contributions of all authors. All authors have given approval to the final version of the manuscript.

Notes

The authors declare the following competing financial interest(s): P.J.M. and R.M.M. are listed as co-inventors on several (provisional) patents related to MOFs.

ACKNOWLEDGEMENTS

Funding Sources

This research was supported by the National Institute of General Medical Sciences of the National Institutes of Health under award number R35GM138165 (R.M.M., T.A.P., P.J.M.) and the National Science Foundation under award number CHE-2203369 (P.S.L., J.J. Wilson). The content is solely the responsibility of the authors and does not necessarily represent the official views of the National Institutes of Health or National Science Foundation. We acknowledge the support of a Camille Dreyfus Teacher-Scholar Award to PJM (TC-23-048).

Computational works (J.-H.L.) were supported by the KIST Institutional Program (Project No. 2E32531) and the program of Future Hydrogen Original Technology Development (Project No. 2021M3I3A1083946), through the National Research Foundation of Korea (NRF), funded by the Ministry of Science and ICT. Computational resources provided by KISTI Supercomputing Center (Project No. KSC-2021-CRE-0430). Additional support was provided by the American Heart Association Predoctoral Fellowship (J.J. Woods) under award number 20PRE3512039. This work made use of Beamline 11-BM of the Advanced Photon Source. Use of the Advanced Photon Source at Argonne National Laboratory was supported by the U. S. Department of Energy, Office of Science, Office of Basic Energy Sciences, under Contract No. DE-AC02-06CH11357. T.R. acknowledges the support of the Welch Foundation (Grant No. N-2012-20220331).

In addition, the authors would like to thank Prof. Joaquin B. Araos (Cornell Department of Veterinary Medicine) for the donation of the porcine skin used for all transdermal experiments and Sijing Meng (Cornell University) for her help in designing figures.

REFERENCES

- (1) Abe, K.; Kimura, H. The Possible Role of Hydrogen Sulfide as an Endogenous Neuromodulator. *J. Neurosci.* **1996**, *16* (3), 1066–1071. <https://doi.org/10.1523/JNEUROSCI.16-03-01066.1996>.
- (2) Goodwin, L. R.; Francom, D.; Dieken, F. P.; Taylor, J. D.; Warenycia, M. W.; Reiffenstein, R. J.; Dowling, G. Determination of Sulfide in Brain Tissue by Gas Dialysis/Ion Chromatography: Postmortem Studies and Two Case Reports. *J. Anal. Toxicol.* **1989**, *13* (2), 105–109. <https://doi.org/10.1093/jat/13.2.105>.
- (3) Yang, G.; Sener, A.; Ji, Y.; Pei, Y.; Pluth, M. D. Gasotransmitters in Biology and Medicine: Molecular Mechanisms and Drug Targets. *Oxid. Med. Cell. Longev.* **2016**, *2016*, 1–2. <https://doi.org/10.1155/2016/4627308>.
- (4) Filipovic, M. R.; Zivanovic, J.; Alvarez, B.; Banerjee, R. Chemical Biology of H₂S Signaling through Persulfidation. *Chem. Rev.* **2018**, *118* (3), 1253–1337. <https://doi.org/10.1021/acs.chemrev.7b00205>.
- (5) Vandiver, M. S.; Snyder, S. H. Hydrogen Sulfide: A Gasotransmitter of Clinical Relevance. *J. Mol. Med.* **2012**, *90* (3), 255–263. <https://doi.org/10.1007/s00109-012-0873-4>.
- (6) Xu, M.; Zhang, L.; Song, S.; Pan, L.; Muhammad Arslan, I.; Chen, Y.; Yang, S. Hydrogen Sulfide: Recent Progress and Perspectives for the Treatment of Dermatological Diseases. *J. Adv. Res.* **2021**, *27*, 11–17. <https://doi.org/10.1016/j.jare.2020.02.003>.
- (7) Wallace, J. L.; Wang, R. Hydrogen Sulfide-Based Therapeutics: Exploiting a Unique but Ubiquitous Gasotransmitter. *Nat. Rev. Drug Discov.* **2015**, *14* (5), 329–345. <https://doi.org/10.1038/nrd4433>.
- (8) Song, Z.; Zhao, L.; Ma, T.; Osama, A.; Shen, T.; He, Y.; Fang, J. Progress and Perspective on Hydrogen Sulfide Donors and Their Biomedical Applications. *Med. Res. Rev.* **2022**, *42* (5), 1930–1977. <https://doi.org/10.1002/med.21913>.
- (9) Xiao, Q.; Xiong, L.; Tang, J.; Li, L.; Li, L. Hydrogen Sulfide in Skin Diseases: A Novel Mediator and Therapeutic Target. *Oxid. Med. Cell. Longev.* **2021**, *2021*, 1–11. <https://doi.org/10.1155/2021/6652086>.
- (10) Coavoy-Sánchez, S. A.; Costa, S. K. P.; Muscará, M. N. Hydrogen Sulfide and Dermatological Diseases. *Br. J. Pharmacol.* **2020**, *177* (4), 857–865. <https://doi.org/10.1111/bph.14699>.
- (11) Marwah, M. K.; Shokr, H.; Sanchez-Aranguren, L.; Badhan, R. K. S.; Wang, K.; Ahmad, S. Transdermal Delivery of a Hydrogen Sulphide Donor, ADT-OH Using Aqueous Gel Formulations for the Treatment of Impaired Vascular Function: An Ex Vivo Study. *Pharm. Res.* **2022**, *39* (2), 341–352. <https://doi.org/10.1007/s11095-021-03164-z>.
- (12) Marwah, M. K.; Manhoosh, B.; Shokr, H.; Al Tahan, M. A.; Stewart, R.; Iqbal, M.; Sanchez, L. D.; Abdullah, S.; Ahmad, S.; Wang, K.; Rana, K. S.; Sanchez-Aranguren, L. Transdermal Delivery of Mitochondrial-Targeted Hydrogen Sulfide Donor, AP39 Protects against 6-Hydroxydopamine-Induced Mitochondrial Dysfunction. *Eur. J. Pharm. Biopharm.* **2023**, *191*, 166–174. <https://doi.org/10.1016/j.ejpb.2023.09.004>.
- (13) Lu, C.; Li, Y.; Zhu, W.; Yang, Y.; Liu, K.; Li, Q.; Gao, M. A Theranostic Probe for Promotion of Skin Wound Healing by Exudate-Triggered H₂S Release with Self-Monitoring Ability. *ACS Appl. Bio Mater.* **2023**, *6* (2), 674–680. <https://doi.org/10.1021/acsabm.2c00919>.
- (14) Wu, J.; Chen, A.; Zhou, Y.; Zheng, S.; Yang, Y.; An, Y.; Xu, K.; He, H.; Kang, J.; Luckanagul, J. A.; Xian, M.; Xiao, J.; Wang, Q. Novel H₂S-Releasing Hydrogel for Wound Repair via In Situ Polarization of M2 Macrophages. *Biomaterials* **2019**, *222*, 119398. <https://doi.org/10.1016/j.biomaterials.2019.119398>.
- (15) Wu, J.; Li, Y.; He, C.; Kang, J.; Ye, J.; Xiao, Z.; Zhu, J.; Chen, A.; Feng, S.; Li, X.; Xiao, J.; Xian, M.; Wang, Q. Novel H₂S Releasing Nanofibrous Coating for In Vivo Dermal Wound Regeneration. *ACS Appl. Mater. Interfaces* **2016**, *8* (41), 27474–27481. <https://doi.org/10.1021/acsami.6b06466>.
- (16) Zhao, X.; Liu, L.; An, T.; Xian, M.; Luckanagul, J. A.; Su, Z.; Lin, Y.; Wang, Q. A Hydrogen Sulfide-Releasing Alginate Dressing for Effective Wound Healing. *Acta Biomater.* **2020**, *104*, 85–94. <https://doi.org/10.1016/j.actbio.2019.12.032>.
- (17) Yuan, F.; He, X.; Lu, Y.; Ning, L.; Zhao, X.; Zhang, S.; Guan, F.; Guo, Y.; Zhang, J. Photoactivated Hydrogen Sulfide Donor with a Near-Infrared Fluorescence Report System for Accelerated Chronic Wound Healing. *Anal. Chem.* **2023**, *95* (17), 6931–6939. <https://doi.org/10.1021/acs.analchem.3c00230>.
- (18) Han, X.; Wang, L.; Shang, Y.; Liu, X.; Yuan, J.; Shen, J. Hydrogen Sulfide-Releasing Polyurethane/Gelatin/Keratin-TA Conjugate Mats for Wound Healing. *J. Mater. Chem. B* **2022**, *10* (42), 8672–8683. <https://doi.org/10.1039/D2TB01700H>.
- (19) Lin, W.-C.; Huang, C.-C.; Lin, S.-J.; Li, M.-J.; Chang, Y.; Lin, Y.-J.; Wan, W.-L.; Shih, P.-C.; Sung, H.-W. In Situ Depot Comprising Phase-Change Materials That Can Sustainably Release a Gasotransmitter H₂S to Treat Diabetic Wounds. *Biomaterials* **2017**, *145*, 1–8. <https://doi.org/10.1016/j.biomaterials.2017.08.023>.
- (20) Lian, J.; Ju, G.; Cai, X.; Cai, Y.; Li, C.; Ma, S.; Cao, Y. Nanofibrous Membrane Dressings Loaded With Sodium

(21) Hydrogen Sulfide/Endothelial Progenitor Cells Promote Wound Healing. *Front. Bioeng. Biotechnol.* **2021**, *9*, 657549. <https://doi.org/10.3389/fbioe.2021.657549>.

(22) Powell, C. R.; Dillon, K. M.; Matson, J. B. A Review of Hydrogen Sulfide (H_2S) Donors: Chemistry and Potential Therapeutic Applications. *Biochem. Pharmacol.* **2018**, *149*, 110–123. <https://doi.org/10.1016/j.bcp.2017.11.014>.

(23) Shi, X.; Li, H.; Guo, F.; Li, D.; Xu, F. Novel Ray of Hope for Diabetic Wound Healing: Hydrogen Sulfide and Its Releasing Agents. *J. Adv. Res.* **2023**, S2090123223001467. <https://doi.org/10.1016/j.jare.2023.05.009>.

(24) Caliendo, G.; Cirino, G.; Santagada, V.; Wallace, J. L. Synthesis and Biological Effects of Hydrogen Sulfide (H_2S): Development of H_2S -Releasing Drugs as Pharmaceuticals. *J. Med. Chem.* **2010**, *53* (17), 6275–6286. <https://doi.org/10.1021/jm901638j>.

(25) DeLeon, E. R.; Stoy, G. F.; Olson, K. R. Passive Loss of Hydrogen Sulfide in Biological Experiments. *Anal. Biochem.* **2012**, *421* (1), 203–207. <https://doi.org/10.1016/j.ab.2011.10.016>.

(26) Kashfi, K.; Olson, K. R. Biology and Therapeutic Potential of Hydrogen Sulfide and Hydrogen Sulfide-Releasing Chimeras. *Biochem. Pharmacol.* **2013**, *85* (5), 689–703. <https://doi.org/10.1016/j.bcp.2012.10.019>.

(27) Xie, X.; Dai, H.; Zhuang, B.; Chai, L.; Xie, Y.; Li, Y. Exogenous Hydrogen Sulfide Promotes Cell Proliferation and Differentiation by Modulating Autophagy in Human Keratinocytes. *Biochem. Biophys. Res. Commun.* **2016**, *472* (3), 437–443. <https://doi.org/10.1016/j.bbrc.2016.01.047>.

(28) Gobbi, G.; Ricci, F.; Malinverno, C.; Carubbi, C.; Pambianco, M.; Panfilis, G. D.; Vitale, M.; Mirandola, P. Hydrogen Sulfide Impairs Keratinocyte Cell Growth and Adhesion Inhibiting Mitogen-Activated Protein Kinase Signaling. *Lab. Invest.* **2009**, *89* (9), 994–1006. <https://doi.org/10.1038/labinvest.2009.61>.

(29) Wang, X.-L.; Tian, B.; Huang, Y.; Peng, X.-Y.; Chen, L.-H.; Li, J.-C.; Liu, T. Hydrogen Sulfide-Induced Itch Requires Activation of Cav3.2 T-Type Calcium Channel in Mice. *Sci. Rep.* **2015**, *5* (1), 16768. <https://doi.org/10.1038/srep16768>.

(30) Whiteman, M.; Li, L.; Rose, P.; Tan, C.-H.; Parkinson, D. B.; Moore, P. K. The Effect of Hydrogen Sulfide Donors on Lipopolysaccharide-Induced Formation of Inflammatory Mediators in Macrophages. *Antioxid. Redox Signal.* **2010**, *12* (10), 1147–1154. <https://doi.org/10.1089/ars.2009.2899>.

(31) Chen, F. E.; Mandel, R. M.; Woods, J. J.; Lee, J.-H.; Kim, J.; Hsu, J. H.; Fuentes-Rivera, J. J.; Wilson, J. J.; Milner, P. J. Biocompatible Metal–Organic Frameworks for the Storage and Therapeutic Delivery of Hydrogen Sulfide. *Chem. Sci.* **2021**, *12* (22), 7848–7857. <https://doi.org/10.1039/D1SC00691F>.

(32) He, S.; Wu, L.; Li, X.; Sun, H.; Xiong, T.; Liu, J.; Huang, C.; Xu, H.; Sun, H.; Chen, W.; Gref, R.; Zhang, J. Metal–Organic Frameworks for Advanced Drug Delivery. *Acta Pharm. Sin. B* **2021**, *11* (8), 2362–2395. <https://doi.org/10.1016/j.apsb.2021.03.019>.

(33) Taherzade, S. D.; Rojas, S.; Soleimannejad, J.; Horcajada, P. Combined Cutaneous Therapy Using Biocompatible Metal–Organic Frameworks. *Nanomaterials* **2020**, *10* (12), 2296. <https://doi.org/10.3390/nano10122296>.

(34) Mallakpour, S.; Nikkhoo, E.; Hussain, C. M. Application of MOF Materials as Drug Delivery Systems for Cancer Therapy and Dermal Treatment. *Coord. Chem. Rev.* **2022**, *451*, 214262. <https://doi.org/10.1016/j.ccr.2021.214262>.

(35) Maranescu, B.; Visa, A. Applications of Metal–Organic Frameworks as Drug Delivery Systems. *Int. J. Mol. Sci.* **2022**, *23* (8), 4458. <https://doi.org/10.3390/ijms23084458>.

(36) Hoshyar, N.; Gray, S.; Han, H.; Bao, G. The Effect of Nanoparticle Size on *in Vivo* Pharmacokinetics and Cellular Interaction. *Nanomed.* **2016**, *11* (6), 673–692. <https://doi.org/10.2217/nnm.16.5>.

(37) Márquez, A. G.; Hidalgo, T.; Lana, H.; Cunha, D.; Blanco-Prieto, M. J.; Álvarez-Lorenzo, C.; Boissière, C.; Sánchez, C.; Serre, C.; Horcajada, P. Biocompatible Polymer–Metal–Organic Framework Composite Patches for Cutaneous Administration of Cosmetic Molecules. *J. Mater. Chem. B* **2016**, *4* (43), 7031–7040. <https://doi.org/10.1039/C6TB01652A>.

(38) Rojas, S.; Colinet, I.; Cunha, D.; Hidalgo, T.; Salles, F.; Serre, C.; Guillou, N.; Horcajada, P. Towards Understanding Drug Incorporation and Delivery from Biocompatible Metal–Organic Frameworks in View of Cutaneous Administration. *ACS Omega* **2018**, *3* (3), 2994–3003. <https://doi.org/10.1021/acsomega.8b00185>.

(39) Rojas, S.; Wheatley, P. S.; Quartapelle-Procopio, E.; Gil, B.; Marszalek, B.; Morris, R. E.; Barea, E. Metal–Organic Frameworks as Potential Multi-Carriers of Drugs. *CrystEngComm* **2013**, *15* (45), 9364. <https://doi.org/10.1039/c3ce41289j>.

(40) Rojas, S.; Horcajada, P. Understanding the Incorporation and Release of Salicylic Acid in Metal–Organic Frameworks for Topical Administration. *Eur. J. Inorg. Chem.* **2021**, *2021* (14), 1325–1331. <https://doi.org/10.1002/ejic.202001134>.

(41) Osorio-Toribio, G.; Velásquez-Hernández, M. D. J.; Mileo, P. G. M.; Zárate, J. A.; Aguilera-Rosas, J.; Leyva-Gómez, G.; Sánchez-Sánchez, R.; Magaña, J. J.; Pérez-Díaz, M. A.; Lázaro, I. A.; Forgan, R. S.; Maurin, G.; Lima, E.; Ibarra, I. A. Controlled Transdermal Release of Antioxidant Ferulate by a Porous Sc(III) MOF. *iScience* **2020**, *23* (6), 101156. <https://doi.org/10.1016/j.isci.2020.101156>.

(42) Huang, X.; Brazel, C. S. On the Importance and Mechanisms of Burst Release in Matrix-Controlled Drug Delivery Systems. *J. Controlled Release* **2001**, *73* (2–3), 121–136. [https://doi.org/10.1016/S0168-3659\(01\)00248-6](https://doi.org/10.1016/S0168-3659(01)00248-6).

(43) Yao, S.; Wang, Y.; Chi, J.; Yu, Y.; Zhao, Y.; Luo, Y.; Wang, Y. Porous MOF Microneedle Array Patch with Photothermal Responsive Nitric Oxide Delivery for Wound Healing. *Adv. Sci.* **2022**, *9* (3), 2103449. <https://doi.org/10.1002/advs.202103449>.

(44) Zhang, P.; Li, Y.; Tang, Y.; Shen, H.; Li, J.; Yi, Z.; Ke, Q.; Xu, H. Copper-Based Metal–Organic Framework as a Controllable Nitric Oxide-Releasing Vehicle for Enhanced Diabetic Wound Healing. *ACS Appl. Mater. Interfaces* **2020**, *12* (16), 18319–18331. <https://doi.org/10.1021/acsami.0c01792>.

(44) Lin, J.; Ho, W.; Qin, X.; Leung, C.; Au, V. K.; Lee, S. Metal-Organic Frameworks for NO_x Adsorption and Their Applications in Separation, Sensing, Catalysis, and Biology. *Small* **2022**, *18* (13), 2105484. <https://doi.org/10.1002/smll.202105484>.

(45) Diring, S.; Carné-Sánchez, A.; Zhang, J.; Ikemura, S.; Kim, C.; Inaba, H.; Kitagawa, S.; Furukawa, S. Light Responsive Metal-Organic Frameworks as Controllable CO-Releasing Cell Culture Substrates. *Chem. Sci.* **2017**, *8* (3), 2381–2386. <https://doi.org/10.1039/C6SC04824B>.

(46) Ma, M.; Noei, H.; Mienert, B.; Niesel, J.; Bill, E.; Muhler, M.; Fischer, R. A.; Wang, Y.; Schatzschneider, U.; Metzler-Nolte, N. Iron Metal-Organic Frameworks MIL-88B and NH_2 -MIL-88B for the Loading and Delivery of the Gas-transmitter Carbon Monoxide. *Chem. – Eur. J.* **2013**, *19* (21), 6785–6790. <https://doi.org/10.1002/chem.201201743>.

(47) Silva, A. F.; Calhau, I. B.; Gomes, A. C.; Valente, A. A.; Gonçalves, I. S.; Pillinger, M. Tricarbonyl-Pyrazine-Molybdenum(0) Metal-Organic Frameworks for the Storage and Delivery of Biologically Active Carbon Monoxide. *ACS Biomater. Sci. Eng.* **2023**, *9* (4), 1909–1918. <https://doi.org/10.1021/acsbiomaterials.3c00140>.

(48) Allan, P. K.; Wheatley, P. S.; Aldous, D.; Mohideen, M. I.; Tang, C.; Hriljac, J. A.; Megson, I. L.; Chapman, K. W.; De Weireld, G.; Vaesen, S.; Morris, R. E. Metal-Organic Frameworks for the Storage and Delivery of Biologically Active Hydrogen Sulfide. *Dalton Trans.* **2012**, *41* (14), 4060. <https://doi.org/10.1039/c2dt12069k>.

(49) Tonzetich, Z. J. H_2S and Bioinorganic Metal Complexes. In *Hydrogen Sulfide*; Pluth, M. D., Ed.; Wiley, 2022; pp 103–141. <https://doi.org/10.1002/9781119799900.ch5>.

(50) Woods, J. J.; Wilson, J. J. Bioinorganic Chemistry of Hydrogen Sulfide: Detection, Delivery, and Interactions with Metalloproteins. In *Encyclopedia of Inorganic and Bioinorganic Chemistry*; Scott, R. A., Ed.; Wiley, 2021; pp 1–22. <https://doi.org/10.1002/9781119951438.eibc2764>.

(51) Olas, B. Hydrogen Sulfide in Signaling Pathways. *Clin. Chim. Acta* **2015**, *439*, 212–218. <https://doi.org/10.1016/j.cca.2014.10.037>.

(52) Keasler, K. T.; Zick, M. E.; Stacy, E. E.; Kim, J.; Lee, J.-H.; Aeindartehran, L.; Runčevski, T.; Milner, P. J. Handling Fluorinated Gases as Solid Reagents Using Metal-Organic Frameworks. *Science* **2023**, *381* (6665), 1455–1461. <https://doi.org/10.1126/science.adg8835>.

(53) Kökçam-Demir, Ü.; Goldman, A.; Esrafil, L.; Gharib, M.; Morsali, A.; Weingart, O.; Janiak, C. Coordinatively Unsaturated Metal Sites (Open Metal Sites) in Metal-Organic Frameworks: Design and Applications. *Chem. Soc. Rev.* **2020**, *49* (9), 2751–2798. <https://doi.org/10.1039/C9CS00609E>.

(54) Martínez-Ahumada, E.; Díaz-Ramírez, M. L.; Velásquez-Hernández, M. D. J.; Jancik, V.; Ibarra, I. A. Capture of Toxic Gases in MOFs: SO_2 , H_2S , NH_3 and NO_x . *Chem. Sci.* **2021**, *12* (20), 6772–6799. <https://doi.org/10.1039/D1SC01609A>.

(55) Liu, J.; Wei, Y.; Li, P.; Zhao, Y.; Zou, R. Selective $\text{H}_2\text{S}/\text{CO}_2$ Separation by Metal-Organic Frameworks Based on Chemical-Physical Adsorption. *J. Phys. Chem. C* **2017**, *121* (24), 13249–13255. <https://doi.org/10.1021/acs.jpcc.7b04465>.

(56) Obeso, J. L.; Amaro, D. R.; Flores, C. V.; Gutiérrez-Alejandro, A.; Peralta, R. A.; Leyva, C.; Ibarra, I. A. Chemical Transformations of Highly Toxic H_2S to Promising Clean Energy in MOFs. *Coord. Chem. Rev.* **2023**, *485*, 215135. <https://doi.org/10.1016/j.ccr.2023.215135>.

(57) Martínez-Ahumada, E.; López-Olvera, A.; Jancik, V.; Sánchez-Bautista, J. E.; González-Zamora, E.; Martis, V.; Williams, D. R.; Ibarra, I. A. MOF Materials for the Capture of Highly Toxic H_2S and SO_2 . *Organometallics* **2020**, *39* (7), 883–915. <https://doi.org/10.1021/acs.organomet.9b00735>.

(58) Li, Y. Research Progress of Hydrogen Sulfide Adsorption Based on MOFs. *ChemistrySelect* **2021**, *6* (37), 9960–9968. <https://doi.org/10.1002/slct.202102950>.

(59) Georgiadis, A. G.; Charisiou, N.; Yentekakis, I. V.; Goula, M. A. Hydrogen Sulfide (H_2S) Removal via MOFs. *Materials* **2020**, *13* (16), 3640. <https://doi.org/10.3390/ma13163640>.

(60) Joshi, J. N.; Zhu, G.; Lee, J. J.; Carter, E. A.; Jones, C. W.; Lively, R. P.; Walton, K. S. Probing Metal-Organic Framework Design for Adsorptive Natural Gas Purification. *Langmuir* **2018**, *34* (29), 8443–8450. <https://doi.org/10.1021/acs.langmuir.8b00889>.

(61) Sánchez-González, E.; Mileo, P. G. M.; Sagastuy-Breña, M.; Álvarez, J. R.; Reynolds, J. E.; Villarreal, A.; Gutiérrez-Alejandro, A.; Ramírez, J.; Balmaseda, J.; González-Zamora, E.; Maurin, G.; Humphrey, S. M.; Ibarra, I. A. Highly Reversible Sorption of H_2S and CO_2 by an Environmentally Friendly Mg-Based MOF. *J. Mater. Chem. A* **2018**, *6* (35), 16900–16909. <https://doi.org/10.1039/C8TA05400B>.

(62) Hamon, L.; Leclerc, H.; Ghoufi, A.; Oliviero, L.; Travert, A.; Lavalley, J.-C.; Devic, T.; Serre, C.; Férey, G.; De Weireld, G.; Vimont, A.; Maurin, G. Molecular Insight into the Adsorption of H_2S in the Flexible MIL-53(Cr) and Rigid MIL-47(V) MOFs: Infrared Spectroscopy Combined to Molecular Simulations. *J. Phys. Chem. C* **2011**, *115* (5), 2047–2056. <https://doi.org/10.1021/jp1092724>.

(63) Hamon, L.; Serre, C.; Devic, T.; Loiseau, T.; Millange, F.; Férey, G.; Weireld, G. D. Comparative Study of Hydrogen Sulfide Adsorption in the MIL-53(Al, Cr, Fe), MIL-47(V), MIL-100(Cr), and MIL-101(Cr) Metal-Organic Frameworks at Room Temperature. *J. Am. Chem. Soc.* **2009**, *131* (25), 8775–8777. <https://doi.org/10.1021/ja901587t>.

(64) Zárate, J. A.; Sánchez-González, E.; Jurado-Vázquez, T.; Gutiérrez-Alejandro, A.; González-Zamora, E.; Castillo, I.; Maurin, G.; Ibarra, I. A. Outstanding Reversible H_2S Capture by an Al(III)-Based MOF. *Chem. Commun.* **2019**, *55* (21), 3049–3052. <https://doi.org/10.1039/C8CC09379B>.

(65) Nguyen-Thuy, T.; Le-Hoang, P.; Hoang Vu, N.; Le, T. N.-M.; Le Hoang Doan, T.; Kuo, J.-L.; Nguyen, T. T.; Phan, T. B.; Nguyen-Manh, D. Hydrogen Adsorption Mechanism of MOF-74 Metal-Organic Frameworks: An Insight from First Principles Calculations. *RSC Adv.* **2020**, *10* (72), 43940–43949. <https://doi.org/10.1039/D0RA08864A>.

(66) Queen, W. L.; Hudson, M. R.; Bloch, E. D.; Mason, J. A.; Gonzalez, M. I.; Lee, J. S.; Gygi, D.; Howe, J. D.; Lee, K.; Darwisch, T. A.; James, M.; Peterson, V. K.; Teat, S. J.; Smit, B.; Neaton, J. B.; Long, J. R.; Brown, C. M. Comprehensive

Study of Carbon Dioxide Adsorption in the Metal–Organic Frameworks $M_2(dobdc)$ ($M = Mg, Mn, Fe, Co, Ni, Cu, Zn$). *Chem. Sci.* **2014**, *5* (12), 4569–4581. <https://doi.org/10.1039/C4SC02064B>.

(67) Rosi, N. L.; Kim, J.; Eddaoudi, M.; Chen, B.; O’Keeffe, M.; Yaghi, O. M. Rod Packings and Metal–Organic Frameworks Constructed from Rod-Shaped Secondary Building Units. *J. Am. Chem. Soc.* **2005**, *127* (5), 1504–1518. <https://doi.org/10.1021/ja045123o>.

(68) Lawson, S.; Rownaghi, A. A.; Rezaei, F. Combined Ibuprofen and Curcumin Delivery Using Mg-MOF-74 as a Single Nanocarrier. *ACS Appl. Bio Mater.* **2022**, *5* (1), 265–271. <https://doi.org/10.1021/acsabm.1c01067>.

(69) Kapelewski, M. T.; Geier, S. J.; Hudson, M. R.; Stück, D.; Mason, J. A.; Nelson, J. N.; Xiao, D. J.; Hulvey, Z.; Gilmour, E.; FitzGerald, S. A.; Head-Gordon, M.; Brown, C. M.; Long, J. R. $M_2(m\text{-}dobdc)$ ($M = Mg, Mn, Fe, Co, Ni$) Metal–Organic Frameworks Exhibiting Increased Charge Density and Enhanced H₂ Binding at the Open Metal Sites. *J. Am. Chem. Soc.* **2014**, *136* (34), 12119–12129. <https://doi.org/10.1021/ja506230r>.

(70) Chen, E. Y.; Mandel, R. M.; Milner, P. J. Evaluating Solvothermal and Mechanochemical Routes towards the Metal–Organic Framework $Mg_2(m\text{-}dobdc}$. *CrystEngComm* **2022**, *24* (41), 7292–7297. <https://doi.org/10.1039/D2CE00739H>.

(71) Rieth, A. J.; Tulchinsky, Y.; Dincă, M. High and Reversible Ammonia Uptake in Mesoporous Azolate Metal–Organic Frameworks with Open Mn, Co, and Ni Sites. *J. Am. Chem. Soc.* **2016**, *138* (30), 9401–9404. <https://doi.org/10.1021/jacs.6b05723>.

(72) Colombo, V.; Galli, S.; Choi, H. J.; Han, G. D.; Maspero, A.; Palmisano, G.; Masciocchi, N.; Long, J. R. High Thermal and Chemical Stability in Pyrazolate-Bridged Metal–Organic Frameworks with Exposed Metal Sites. *Chem. Sci.* **2011**, *2* (7), 1311. <https://doi.org/10.1039/c1sc00136a>.

(73) Wang, Z.; Bilegsaikhan, A.; Jerozal, R. T.; Pitt, T. A.; Milner, P. J. Evaluating the Robustness of Metal–Organic Frameworks for Synthetic Chemistry. *ACS Appl. Mater. Interfaces* **2021**, *13* (15), 17517–17531. <https://doi.org/10.1021/acsami.1c01329>.

(74) Chen, F. E.; Pitt, T. A.; Okong’o, D. J.; Wetherbee, L. G.; Fuentes-Rivera, J. J.; Milner, P. J. A Structure–Activity Study of Aromatic Acid Modulators for the Synthesis of Zirconium-Based Metal–Organic Frameworks. *Chem. Mater.* **2022**, *34* (7), 3383–3394. <https://doi.org/10.1021/acs.chemmater.2c00241>.

(75) Rieth, A. J.; Wright, A. M.; Dincă, M. Kinetic Stability of Metal–Organic Frameworks for Corrosive and Coordinating Gas Capture. *Nat. Rev. Mater.* **2019**, *4* (11), 708–725. <https://doi.org/10.1038/s41578-019-0140-1>.

(76) Fantauzzi, M.; Elsener, B.; Atzei, D.; Rigoldi, A.; Rossi, A. Exploiting XPS for the Identification of Sulfides and Poly-sulfides. *RSC Adv.* **2015**, *5* (93), 75953–75963. <https://doi.org/10.1039/C5RA14915K>.

(77) Ahlström, M. G.; Thyssen, J. P.; Wennervaldt, M.; Menné, T.; Johansen, J. D. Nickel Allergy and Allergic Contact Dermatitis: A Clinical Review of Immunology, Epidemiology, Exposure, and Treatment. *Contact Dermatitis* **2019**, *81* (4), 227–241. <https://doi.org/10.1111/cod.13327>.

(78) Chavan, S.; Bonino, F.; Valenzano, L.; Civalleri, B.; Lamberti, C.; Acerbi, N.; Cavka, J. H.; Leistner, M.; Bordiga, S. Fundamental Aspects of H₂S Adsorption on CPO-27-Ni. *J. Phys. Chem. C* **2013**, *117* (30), 15615–15622. <https://doi.org/10.1021/jp402440u>.

(79) Ying, J.; Wang, Q.; Jiang, M.; Wang, X.; Liu, W.; Wang, X.; Zhang, C.; Xiang, L. Hydrogen Sulfide Promotes Cell Proliferation and Melanin Synthesis in Primary Human Epidermal Melanocytes. *Skin Pharmacol. Physiol.* **2020**, *33* (2), 61–68. <https://doi.org/10.1159/000506818>.

(80) Yang, C.; Yang, Z.; Zhang, M.; Dong, Q.; Wang, X.; Lan, A.; Zeng, F.; Chen, P.; Wang, C.; Feng, J. Hydrogen Sulfide Protects against Chemical Hypoxia-Induced Cytotoxicity and Inflammation in HaCaT Cells through Inhibition of ROS/NF-κB/COX-2 Pathway. *PLoS ONE* **2011**, *6* (7), e21971. <https://doi.org/10.1371/journal.pone.0021971>.

(81) Mosmann, T. Rapid Colorimetric Assay for Cellular Growth and Survival: Application to Proliferation and Cytotoxicity Assays. *J. Immunol. Methods* **1983**, *65* (1–2), 55–63. [https://doi.org/10.1016/0022-1759\(83\)90303-4](https://doi.org/10.1016/0022-1759(83)90303-4).

(82) Burnett, S.; Ferns, R.; Cordes, D. B.; Slawin, A. M. Z.; Van Mourik, T.; Stasch, A. Low-Coordinate Magnesium Sulfide and Selenide Complexes. *Inorg. Chem.* **2023**, *62* (40), 16443–16450. <https://doi.org/10.1021/acs.inorgchem.3c02132>.

(83) Chadwick, S.; Englich, U.; Senge, M. O.; Noll, B. C.; Ruhlandt-Senge, K. Novel Structural Principles in Magnesium Thiolate Chemistry: Monomers, Trimers, and the First Magnesiate Thiolate. *Organometallics* **1998**, *17* (14), 3077–3086. <https://doi.org/10.1021/om980012h>.

(84) Ruhlandt-Senge, K. Synthesis and Characterization of the First Three-Coordinate Donor-Free Magnesium Thiolates, $[Mg(STriph)_2]_2$ (Triph = 2,4,6-Ph₃C₆H₂) and $[Mg(SMes^*)_2]_2$ (Mes* = 2,4,6-t-Bu₃C₆H₂), and the Four-Coordinate Magnesium Thiolate $Mg(SMes^*)_2(OEt_2)_2$ and Selenolate $Mg(SeMes^*)_2(\text{THF})_2$. *Inorg. Chem.* **1995**, *34* (13), 3499–3504. <https://doi.org/10.1021/ic00117a019>.

(85) Ren, W.; Gu, D. An Azobenzoyl Anion Radical Complex of Magnesium: Synthesis, Structure, and Reactivity Studies. *Inorg. Chem.* **2016**, *55* (22), 11962–11970. <https://doi.org/10.1021/acs.inorgchem.6b02114>.

(86) Janssen, M. D.; Van Der Rijst, R.; Spek, A. L.; Grove, D. M.; Van Koten, G. Synthesis and Characterization of Bis(Arenethiolato)Magnesium Complexes with Intramolecular Coordination. X-Ray Structure of $[Mg\{S(C_6H_4\text{-}2\text{-}CH}_2\text{NMe}_2)\}_2]_2$. *Inorg. Chem.* **1996**, *35* (11), 3436–3439. <https://doi.org/10.1021/ic951288+>.

(87) Lelj, F. Formation, Crystal Structure and Co-Ordination Chemistry of the $[\text{MnIII}(\text{Oespz})(\text{SH})]^-$ [$\text{Oespz}^{2-} = 2,3,7,8,12,13,17,18\text{-Octakis(Ethylsulfanyl)-5,10,15,20-Tetraazaporphyrinate Dianion}$] Complex. *J. Chem. Soc. Dalton Trans.* **1998**, No. 12, 1985–1992. <https://doi.org/10.1039/a708033f>.

(88) Esteruelas, M. A.; Fernández, I.; García-Yebra, C.; Martín, J.; Oñate, E. Cycloosmathioborane Compounds: Other Manifestations of the Hückel Aromaticity. *Inorg. Chem.* **2019**, *58* (4), 2265–2269. <https://doi.org/10.1021/acs.inorgchem.8b03366>.

(89) Sellmann, D.; Lechner, P.; Knoch, F.; Moll, M. Transition-Metal Complexes with Sulfur Ligands. 82. Hydrogen Sulfide, Disulfur, and Carbon Disulfide Molecules as Ligands in Sulfur-Rich $[\text{Ru}(\text{PPh}_3)(\text{S}^4)]$ Complexes [$[\text{S}^4]^{2-} = 1,2\text{-Bis}[(2\text{-Mercaptophenyl})\text{Thio}]\text{Ethane}(2\text{-})$]. *J. Am. Chem. Soc.* **1992**, *114* (3), 922–930. <https://doi.org/10.1021/ja00029a020>.

(90) Chandrika, D.; Ma, E. S.; Rettig, S. J.; James, B. R.; Cullen, W. R. Synthesis and X-Ray Structure of an H_2S Complex, $\text{RuCl}_2(\text{P-N})(\text{P}(p\text{-Tolyl})_3)(\text{SH}_2)$ ($\text{P-N} = o\text{-}(2\text{-Diphenylphosphino)-}N,N\text{-Dimethylaniline}$). *Inorg. Chem.* **1997**, *36* (24), 5426–5427. <https://doi.org/10.1021/ic9707772>.

(91) Ma, E. S. F.; Rettig, S. J.; James, B. R. Extension of the Karplus Relationship to Vicinal Coupling within the P-Ru-S-H Moiety of the H_2S Complexes Cis- $\text{RuX}_2(\text{P-N})(\text{PPh}_3)(\text{SH}_2)$ {X = Cl, Br; P-N = [o-(N,N-Dimethylamino)Phenyl]Diphenylphosphine}. *Chem. Commun.* **1999**, No. 24, 2463–2464. <https://doi.org/10.1039/a907360d>.

(92) Chatwin, S. L.; Diggle, R. A.; Jazzaar, R. F. R.; Macgregor, S. A.; Mahon, M. F.; Whittlesey, M. K. Structure, Reactivity, and Computational Studies of a Novel Ruthenium Hydrogen Sulfide Dihydride Complex. *Inorg. Chem.* **2003**, *42* (24), 7695–7697. <https://doi.org/10.1021/ic030241i>.

(93) Dietzel, P. D. C.; Morita, Y.; Blom, R.; Fjellvåg, H. An In Situ High-Temperature Single-Crystal Investigation of a Dehydrated Metal-Organic Framework Compound and Field-Induced Magnetization of One-Dimensional Metal-Oxygen Chains. *Angew. Chem. Int. Ed.* **2005**, *44* (39), 6354–6358. <https://doi.org/10.1002/anie.200501508>.

(94) Dietzel, P. D. C.; Johnsen, R. E.; Blom, R.; Fjellvåg, H. Structural Changes and Coordinatively Unsaturated Metal Atoms on Dehydration of Honeycomb Analogous Microporous Metal-Organic Frameworks. *Chem. Eur. J.* **2008**, *14* (8), 2389–2397. <https://doi.org/10.1002/chem.200701370>.

(95) Dietzel, P. D. C.; Blom, R.; Fjellvåg, H. Base-Induced Formation of Two Magnesium Metal-Organic Framework Compounds with a Bifunctional Tetratopic Ligand. *Eur. J. Inorg. Chem.* **2008**, *2008* (23), 3624–3632. <https://doi.org/10.1002/ejic.200701284>.

(96) Das, A.; Mandal, P. K.; Lovas, F. J.; Medcraft, C.; Walker, N. R.; Arunan, E. The H_2S Dimer Is Hydrogen-Bonded: Direct Confirmation from Microwave Spectroscopy. *Angew. Chem. Int. Ed.* **2018**, *57* (46), 15199–15203. <https://doi.org/10.1002/anie.201808162>.

(97) Sun, M.; Wang, Y.; Zhang, Q.; Xia, Y.; Ge, W.; Guo, D. Prediction of Reversible Disulfide Based on Features from Local Structural Signatures. *BMC Genomics* **2017**, *18* (1), 279. <https://doi.org/10.1186/s12864-017-3668-8>.

(98) Li, F.; Hanna, G.; Yücesan, G.; Yazaydin, A. O. Functionalization of Metal-Organic Framework Nanochannels for Water Transport and Purification. *ACS Appl. Nano Mater.* **2023**, *6* (4), 3003–3011. <https://doi.org/10.1021/acsanm.2c05389>.

(99) Lin, V. S.; Lippert, A. R.; Chang, C. J. Cell-Trappable Fluorescent Probes for Endogenous Hydrogen Sulfide Signaling and Imaging H_2O_2 -Dependent H_2S Production. *Proc. Natl. Acad. Sci.* **2013**, *110* (18), 7131–7135. <https://doi.org/10.1073/pnas.1302193110>.

(100) Zuluaga, S.; Fuentes-Fernandez, E. M. A.; Tan, K.; Xu, F.; Li, J.; Chabal, Y. J.; Thonhauser, T. Understanding and Controlling Water Stability of MOF-74. *J. Mater. Chem. A* **2016**, *4* (14), 5176–5183. <https://doi.org/10.1039/C5TA10416E>.

(101) Voskanyan, A. A.; Goncharov, V. G.; Novendra, N.; Guo, X.; Navrotsky, A. Thermodynamics Drives the Stability of the MOF-74 Family in Water. *ACS Omega* **2020**, *5* (22), 13158–13163. <https://doi.org/10.1021/acsomega.0c01189>.

(102) Summerfield, A.; Meurens, F.; Ricklin, M. E. The Immunology of the Porcine Skin and Its Value as a Model for Human Skin. *Mol. Immunol.* **2015**, *66* (1), 14–21. <https://doi.org/10.1016/j.molimm.2014.10.023>.

(103) Uhm, C.; Jeong, H.; Lee, S. H.; Hwang, J. S.; Lim, K.-M.; Nam, K. T. Comparison of Structural Characteristics and Molecular Markers of Rabbit Skin, Pig Skin, and Reconstructed Human Epidermis for an Ex Vivo Human Skin Model. *Toxicol. Res.* **2023**, *39* (3), 477–484. <https://doi.org/10.1007/s43188-023-00185-1>.

(104) Lu, H.; Chen, Y.; Hu, P. Current Status and Future Prospects of Hydrogen Sulfide Donor-Based Delivery Systems. *Adv. Ther.* **2023**, *6* (5), 2200349. <https://doi.org/10.1002/adtp.202200349>.

(105) Iciek, M.; Bilska-Wilkoz, A.; Kozdrowicki, M.; Górný, M. Reactive Sulfur Species in Human Diseases. *Antioxid. Redox Signal.* **2023**, *39* (13–15), 1000–1023. <https://doi.org/10.1089/ars.2023.0261>.

(106) Han, Y.; Shang, Q.; Yao, J.; Ji, Y. Hydrogen Sulfide: A Gaseous Signaling Molecule Modulates Tissue Homeostasis: Implications in Ophthalmic Diseases. *Cell Death Dis.* **2019**, *10* (4), 293. <https://doi.org/10.1038/s41419-019-1525-1>.

Insert Table of Contents artwork here

